A statistical investigation of traveling convection vortices observed by the west coast Greenland magnetometer chain

C. Robert Clauer
Space Physics Research Laboratory, University of Michigan, Ann Arbor, Michigan, USA

V. G. Petrov
Space Physics Research Laboratory, University of Michigan, Ann Arbor, Michigan, USA
Institute of Terrestrial Magnetism, Ionosphere, and Radiowave Propagation, Troitsk, Moscow, Russia

Received 24 July 2001; revised 14 January 2002; accepted 14 January 2002; published 30 July 2002.

[1] We report on the results of a statistical investigation of high-latitude traveling ionospheric convection vortices measured by the west coast Greenland magnetometer chain during the year 1996. The events were selected using a data-fitting procedure which identifies vortex-like structures in the ionospheric current distribution. The procedure identified about 22,150 vortices during 1996. For each vortex event, we compute the average value of the current and the average northward and eastward speed, and the standard deviations of the parameters are also computed. We investigate the local time and solar wind dependence of the vortex strength and movement. The solar wind speed appears to be the primary factor which correlates best with the field-aligned current strength related to individual ionospheric vortices. Increasing solar wind speed increases the vortex occurrence, as well as vortex intensity in all dayside local time sectors. The dependence is the strongest in the noon sector, followed by the morning and evening sectors. The interplanetary magnetic field (IMF) B_z component has a nearly comparable influence on vortex strength as the solar wind speed; however, this is observed primarily in the noon sector. The final factor which we have found to correlate with vortex occurrence and strength is the standard deviation of the magnetic field. *INDEX TERMS:* 2409 Ionosphere: Current systems (2708); 2431 Ionosphere: Ionosphere/magnetosphere interactions (2736); 2724 Magnetospheric Physics: Magnetopause, cusp, and boundary layers; 2784 Magnetospheric Physics: Solar wind/magnetosphere interactions; 2708 Magnetospheric Physics: Current systems (2409); *KEYWORDS:* ionosphere, convection, vortex, TCV

1. Introduction

[2] Traveling Convection Vortices (TCVs) form a particular class of high-latitude magnetic pulsation having periods of around 10–30 minutes. The distinguishing characteristic of the pulsation is the spatial distribution of the horizontal disturbance field which is measured by an array of ground magnetometers. The instantaneous perturbation vectors appear to point toward or away from a point source and this source moves across the array with time [*Friis-Christensen et al.*, 1988a, 1988b; *McHenry et al.*, 1990a; *Lühr and Blawert*, 1994]. Such a magnetic signature is consistent with the effect of a circular ionospheric Hall currents associated with a moving field-aligned current interacting with the ionosphere [*McHenry and Clauer*, 1987]. Most investigations of TCVs have been concerned with the so-called impulsive TCV - events which exhibit a transient large magnetic variation with one or two cycles, and generally show an east-west propagation [*Lühr et al.*, 1993; *Lühr and Blawert*, 1994; *Lühr et al.*, 1996; *Glassmeier et al.*, 1989; *Glassmeier and Heppner*, 1992; *Glassmeier*, 1992; *Ridley et al.*, 1998]. A few investigations have been devoted to quasi-continuous or multiple TCV events [*McHenry et al.*, 1990a, 1990b; *Clauer and Ridley*, 1995]. In some cases, however, this division is artificial and is determined only by the selection threshold used for the magnetic perturbation amplitude. While striking in their appearance, large impulsive variations during quiet intervals are infrequent. More often, the impulsive event is an enhanced pulse within an interval of pulsation activity.

[3] Sources of TCVs have been attributed to the compression or decompression of the magnetopause by changes in the solar wind dynamic pressure [*Friis-Christensen et al.*, 1988a; *Sibeck*, 1990], flux transfer events [*Goertz et al.*, 1985; *Lanzerotti et al.*, 1987], Kelvin-Helmholtz instability [*Pu and Kivelson*, 1983; *Clauer and Ridley*, 1995], and plasma injections into low-latitude boundary layer [*Heikkila et al.*, 1989]. Indeed, it is very likely that multiple generation mechanisms exist to produce TCVs. It has been difficult, however, to determine what solar wind parameters may be directly responsible for the observed ground-level TCV disturbances [*Sitar et al.*, 1996; *Sitar and Clauer*, 1999]. Reasons for this include the spatial variability of the

0148-0227/02/2001JA000228

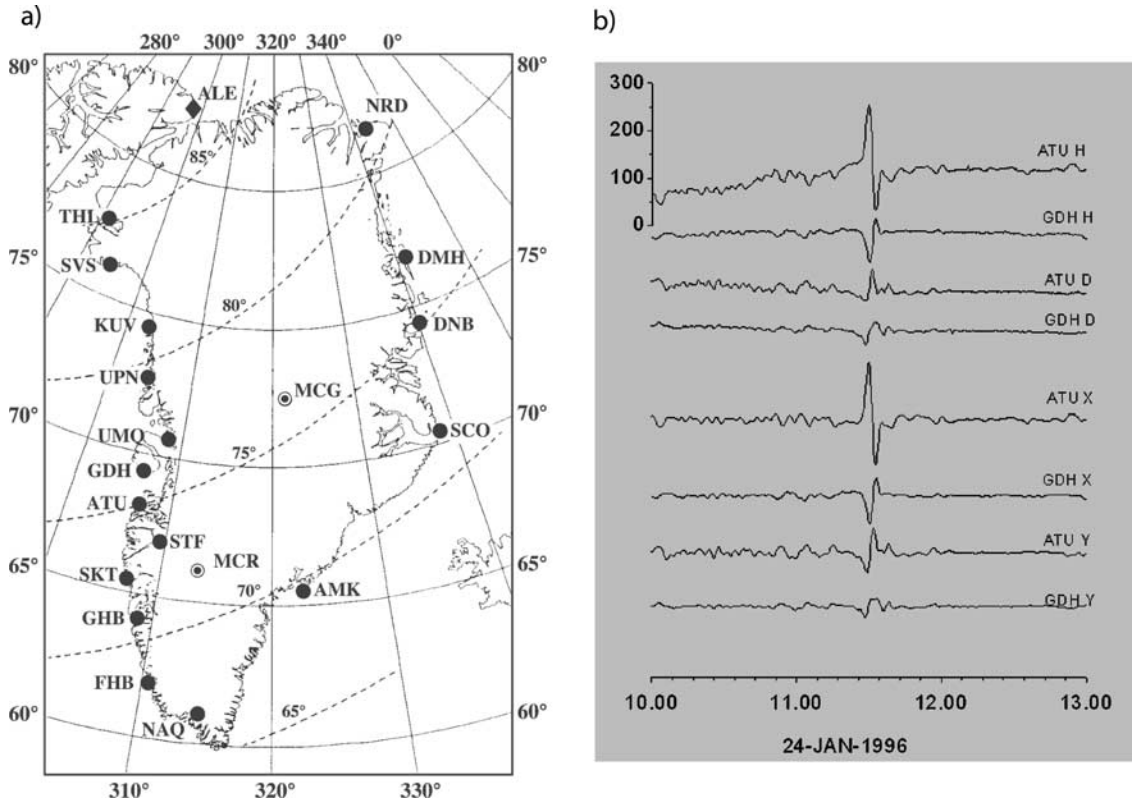

Figure 1. (a) Map of Greenland showing magnetometer stations. Dashed curves show lines of geomagnetic latitude. (b) Traces from stations ATU and GDH showing impulsive TCV event on 24 Jan. 1996. Top curves show the original geomagnetic H-D coordinates, bottom four curves show the filtered and converted to geographic X-Y coordinates.

solar wind parameters and limited spatial coverage of the near Earth upstream region by direct *in situ* measurements, the lack of precise knowledge about the propagation of the solar wind from the spacecraft position to the bow shock and from the bow shock to the magnetopause and to the ionosphere. In addition, *McHenry* [1990a] showed that in some cases sudden change in solar wind parameters can initiate the TCV event which then continues as though self generated. Thus, direct event studies have been difficult and somewhat ambiguous in their ability to establish the relationship between solar wind parameters and ionospheric signatures. Statistical studies have provided results which characterize the impulsive TCVs [*Glassmeier et al.*, 1989; *Lin et al.*, 1995; *Sitar et al.*, 1996; *Sitar and Clauer*, 1999]. However these studies have been based on very limited statistics and each used different criteria to select events, so results are sometimes contradictory and incompatible. Here we undertake a statistical study which is much larger in the amount of data examined and is based on the most common selection criteria–the ground signature of the event must be vortex-like.

2. Methodology

[4] For this statistical study we utilize the 20-second data recorded by the magnetometer stations located along the west coast of Greenland for the entire year 1996. The magnetometer stations lie nearly along a magnetic meridian from a magnetic latitude of about 66° at Narsarsuaq to 86° at Thule. The list of Greenland magnetometer stations are published in [*Clauer and Ridley*, 1995].

[5] Figure 1 shows an example of an isolated vortex event observed on Jan. 24th, 1996 by the Greenland west coast stations. Figure 1a shows a map of Greenland along with the station 3-letter codes. Dashed lines show geographic coordinates and solid lines show magnetic coordinates. The stations along the west coast lie nearly along a magnetic meridian. Data from two Greenland stations, located at the same longitude, but at different latitudes are shown. The duration of the event is about 10 minutes. It is evident from the two upper traces (H-components) that the magnetic perturbations at the two stations have the opposite sense indicating that the current responsible for the perturbations lies between the stations. For the analysis, we convert the data to a local orthogonal cartesian coordinate system centered at Søndre Strømfjord with the $\hat{y}$ positive east along the corrected geomagnetic latitude direction and $\hat{x}$ positive north orthogonal to the corrected geomagnetic latitude. A high pass filter with a 30 minute cutoff has been applied to the data. The four lower traces in Figure 1 display the filtered data converted to the local X-Y orthogonal geomagnetic coordinate system.

[6] To identify TCVs we use an automated approach which is very similar to that developed by *McHenry and Clauer* [1987] and *McHenry et al.* [1990b]. We apply an automated least squares fitting procedure to the filtered data. While *McHenry and Clauer* [1987] and *McHenry et al.* [1990b] fit a model of a filament of field-aligned current

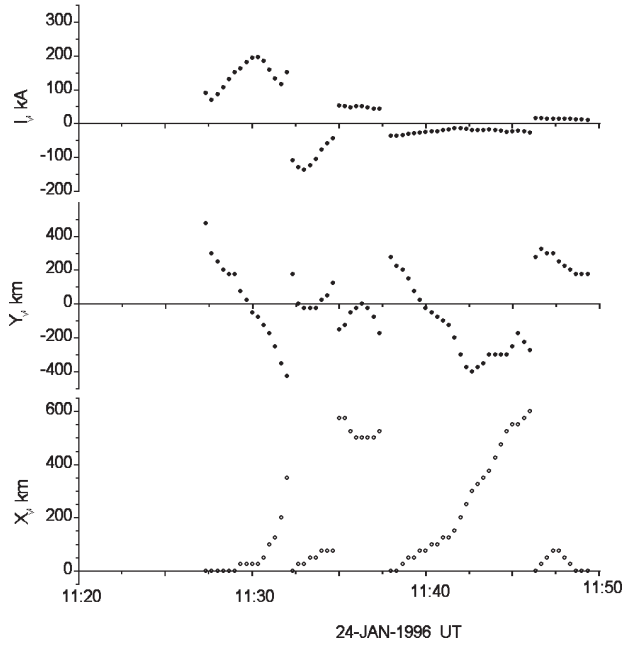

Figure 2. Example of the model fit parameters: field-aligned current (top) and position in Y (middle) and X (bottom).

which spreads to infinity in a uniform conducting ionosphere, we utilize a somewhat more realistic model that limits the size of the ionospheric vortex. We use a coaxial system with upward (downward) field-aligned current along a central cylinder with radius R_1 which closes through downward (upward) current along the external tube with internal radius R_1 and external radius R_2. The current density is constant in the central cylinder and changes linearly from maximum density at R_1 to zero at R_2. This system produces a ring of Hall current with maximum density at $r = R_1$ and zero density at $r = 0$ and $r = R_2$. To calculate the ionospheric current density we use a Hall/Pedersen conductivity ratio of 2. Since the induction effects due to the sea and to the upper conducting layers have been shown to be small for the pulsation periods investigated here [*McHenry*, 1989], we use an idealized model with a perfect conductor at a depth of 350 km [*Banks*, 1969]. To take into account the observed east-west elongation of the TCV current system [*Glassmeier*, 1992], we place together two such field-aligned systems with equal currents separated by a distance D between current centers in the east-west direction. We have estimated the optimum values for R_1, R_2 and D, using a small subset of the data. In general, the double system improves fits over the single system by about 15–30%. The best data fits were found for values of $R_1 = 200$ km, $R_2 = 600$ km, and $D = 300$ km which yields a vortex size of 400 × 700 km, which is consistent with other estimations [*Glassmeier*, 1992].

[7] We do not propose this current system as a model for TCVs, but rather as a tool for the computer automated identification of ionospheric vortices from ground magnetometer data. We compute the magnetic field produced by the model current system at points on the ground and compare with measurements. The parameters of the model are adjusted to minimize the expression:

$$\sigma^2 = \sum_i \left((X_i - I \cdot X(x_v, y_v) - X_0)^2 + (Y_i - I \cdot Y(x_v, y_v) - Y_0)^2 + k_1 \cdot I^2 + k_2 \cdot \left(X_0^2 + Y_0^2\right)\right)$$

where:

X_i, Y_i – measured magnetic field variations at i-station

$X(x_v, y_v)$, $Y(x_v, y_v)$ – the magnetic field created by the model current system with unit current located at point x_v, y_v at the location of the ith station.

I – the value of total field-aligned current

X_0, Y_0 – magnetic field, created by all far away sources (magnetopause and ring current for example) which can be considered as constant for all stations of the chain.

[8] Long period variations are eliminated by filtering the data, however, some short time (<30–40 minutes) variations, which may be produced by distant sources, are not removed and can disturb the results, especially when vortex-like disturbances are small in amplitude. These variations are uniform over the whole chain and are eliminated by X_0 and Y_0. The term $k_1 \cdot I^2 + k_2 \cdot (X_0^2 + Y_0^2)$ is a normalization factor, which is often used in minimization problems to make the results more stable. In our case, it forces a solution with minimum values of I, X_0 and Y_0. Coefficient k_1 and k_2 have been selected experimentally to be $5.0 \cdot 10^{-6}$ and 10 accordingly. The small value of k_1 means that we apply little limitation on I, so obtaining the best fit for this parameter is accomplished without a minimization of I itself. To find the minimum of σ we try all possible positions of the vortex in the range $-700 < x_v < 1500$ and $-900 < y_v < 900$ using 25 km steps. For each pair x_v, y_v, the values of I, X_0, Y_0, which give the minimum of σ can be calculated analytically. Applying this procedure to every 20-sec interval of data, we calculate values of x_v, y_v, I, X_0, Y_0 for every time point. We then exclude points where the model cannot fit the measured magnetic field distribution.

[9] Since the amplitude of the magnetic disturbances varies significantly, we normalize σ by dividing by the average absolute deviation measured by the stations at each time step. If this value is greater than 0.75, we consider the fit inadequate. Points, where the absolute value of the vortex current is less than 20 or greater than 500 kA or the calculated position of vortex is far away from the magnetometer locations ($x_v > 1400$ or $x_v < -600$, $|(y_v)| > 800$) are also excluded as unreliable.

[10] An example of the parameters computed for the Jan. 24th event is presented in Figure 2. We obtain a strong downward current at 11:28–11:32 which produces the positive X-component variation at ATU and negative variation at GDH, moving from east to west with $V_y = -2.8$ km/sec and northward with $V_x = 0.9$ km/sec. We also obtain a train of decaying alternately directed currents moving mainly in the northwest direction. The small second and third vortices show an unstable movement with an average speed that does not exceed one km/sec while showing a large variation in direction. We suppose this is due to the very small distance between the vortices (about 600–700 km) and the magnetic field of the second vortex is disturbed by the stronger field of the first vortex. The single

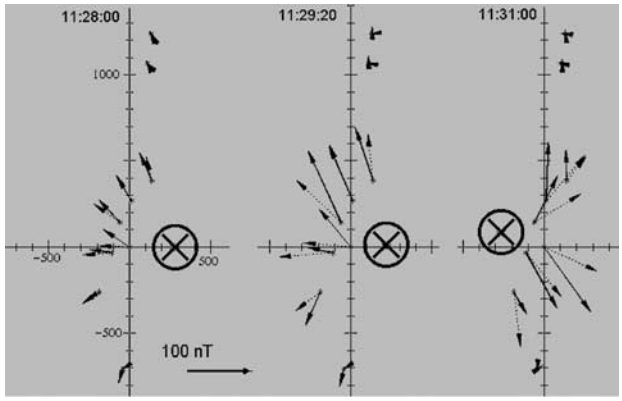

Figure 3. Schematic showing the current location and model magnetic field (dotted lines) and the measurements (solid lines) at the west coast Greenland magnetometer stations converted to local X-Y geomagnetic coordinates.

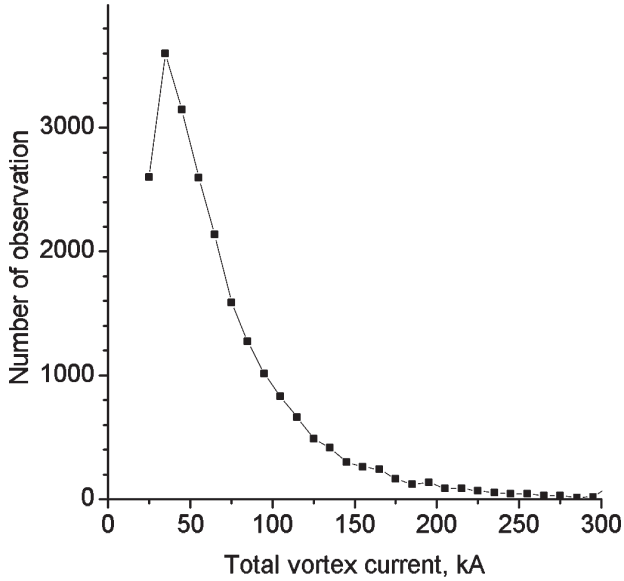

Figure 4. Amplitude distribution of vortex events identified through the application of a computer selection algorithm to Greenland west coast magnetic data for the year 1996.

vortex model does not produce a good estimate of the position of the vortices in such cases. Nevertheless, the model allows us to detect the vortices. Figure 3 shows the position of the vortex (circle), real (solid) and modeled (dotted) magnetic field vectors for a few moments of the 24 Jan. 1996 event. The similarity between the modeled and measured field can be seen and the movement of the vortex is also quite evident.

[11] To undertake the statistical investigation of traveling convection vortices, the data intervals identified by the above procedure were examined to determine the parameters for individual vortices. We accept a vortex identification and associated parameters if there are at least 8 continuous point of data where the variations between each two successive time points are small (variations of I do not exceed 50 kA, variations of x_v, y_v do not exceed 200 km). To ensure that the ionospheric current forms a vortex-like structure, an additional requirement is imposed that stations located northward and southward of the calculated vortex position must have magnetic H-component perturbations of opposite sign. While this restriction sometimes deletes real vortices, it guarantees that all events which are retained are vortex-like. Then for each vortex the average value of the current, and the northward and eastward speed are calculated. To determine the speed, a least square linear fit to the vortex $\hat{x}$ and $\hat{y}$ position as a function of time is done and the slope of this line gives the speed. This procedure produces a list of about 22500 vortices with average current >20 kA, corresponding to magnetic variations greater than about 10 nT, observed between 08–20 UT (06–18 MLT). The amplitude distribution of the events is shown in Figure 4, the distribution of the absolute value of velocities is shown in Figure 5, and Figure 6 shows the distribution of periods, measured as the time between successive vortices multiplied by 2.

[12] Since field line resonances (FLR) also produce a vortex-like ionospheric current, it is necessary to devise a method to distinguish between field-line resonance events and traveling convection vortex events. Distinction of these can be found the period of the pulsations. For field lines at these latitudes (≈75 mlat), typical resonance frequencies lie in the range of 2–4 mHz (8 minute – 4 minute periods) (B. Fraser, personal communication, 2001). From Figure 6 we can see that very few events in our distribution have periods of less than 8 minutes.

[13] The number of vortices used in any given analysis will be governed by the selection criteria. All selection criteria in the work presented here, however, are implemented in computer code and applied to the data so there is no subjective bias in the selection of events. To investigate the relationship between TCVs and the solar wind, we utilize data from the WIND satellite obtained through CDAWeb. The original data have a time resolution of between 1–2 minutes. We compute 20 minute averages for the statistical

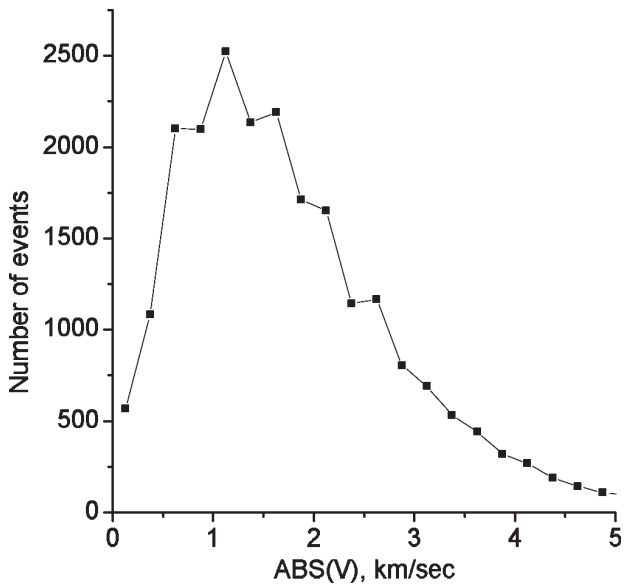

Figure 5. Speed distribution (absolute value of velocity) of vortex events identified through the application of a computer selection algorithm to Greenland west coast magnetic data for the year 1996.

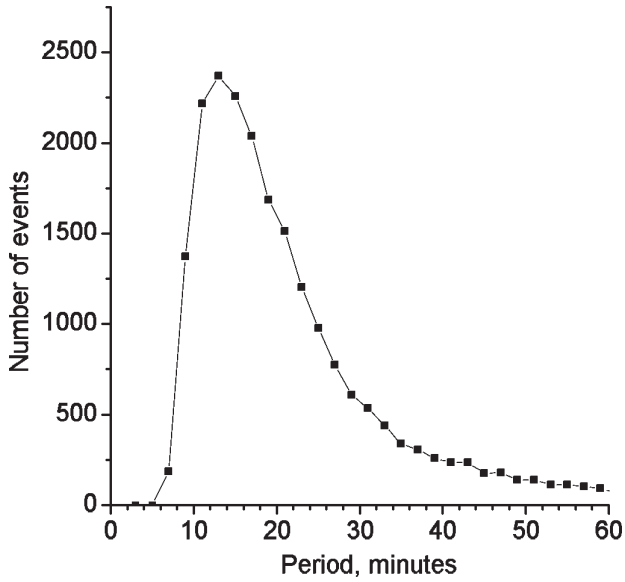

Figure 6. Period distribution of the pulsations which comprise the computer selected TCV events. The period has been determined from the fitted data and is defined to be twice the time separation between two successive vortex centers.

analysis. This choice is based upon the following considerations: First, the average error in determining the propagation time between the satellite and the magnetopause is 7.5 to 8.5 minutes [*Ridley*, 2000]. Second, short time scale variations are not necessarily preserved during the propagation from the WIND location to the magnetopause. Prior to the averaging, the data are checked to remove spikes, since a large spike can significantly affect the average. For each 20 minute interval, we compute the average and standard deviation of the IMF magnetic field components, velocity components, and proton number density. Using the WIND position and average solar wind velocity, the propagation time to the bow shock is calculated. WIND data were available for 315 days during which about 18000 vortices were identified for the statistical analysis.

3 Statistical Results

3.1. Local Time Dependence of Vortex Distribution and Movement

[14] The upper panel of Figure 7 shows the average number of vortices per hour identified during each UT hour in the interval 08–20 UT. This corresponds to magnetic local times ranging from 06–18 MLT (14 MLT is approximately local magnetic noon along the magnetic meridian through the station SFT). The line marked by solid circles shows the statistic for all of the 22500 vortices. Triangles mark the case for vortices with current greater than 50 kA. Imposing this criterion yields 3900 vortices. Both distributions have generally the same shape with a broad maximum between 09–15 MLT with the maximum shifted slightly to the afternoon. In spite of this, however, the total number of morning vortices (between 06–10 MLT) is greater than the number of afternoon vortices (between 14–18 MLT).

[15] The curve for all vortices shows a small decrease between 12–13 UT which is not observed in the curve for the strongest vortices, so we believe that this decrease is not a real feature, but rather the inability of the single vortex model used in our analysis. When vortices follow each other very close and the magnetometers are measuring the total magnetic field of two vortices, our fitting method can become unstable and produce false results, such as fast moving vortices or very distant vortices. As a rule, these are removed due to our selection criterion. Thus, where two closely spaced vortices may be present, we do not even select one. This situation is most likely to occur where the number of vortices per hour is large, i. e., near local noon. Strong vortices, however, are generally not so closely spaced that interference between them affects our fitting and selection procedure.

[16] The middle panel of Figure 7 shows the average northward speed (V_x) of vortices for each UT hour for all events and for large events. In general, both distributions look similar. The average northward speed is about 0.6 km/

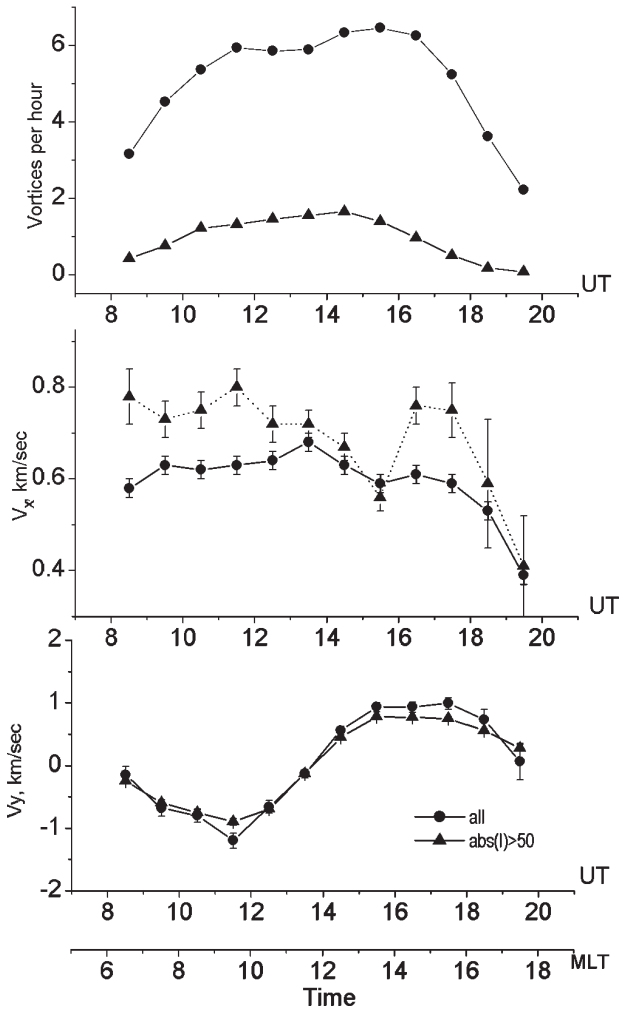

Figure 7. Distribution of the average number of vortices per hour observed as a function of MLT (top) and the average northward (middle) and eastward(bottom) velocity. Circles indicate the average of all events and the triangles indicate the subset of large events.

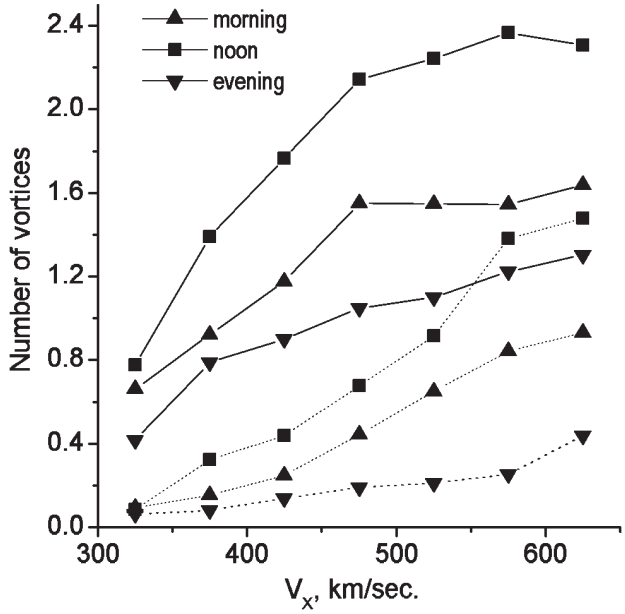

Figure 8. Average number of vortices per 20 minute interval as a function of solar wind velocity V_x divided into morning, noon, and evening sectors. Solid lines indicate the results for the full data set and dotted lines indicate the results for the subset of strong vortices.

sec for all and 0.8 km/sec for the strong vortices in the time interval 8–18 UT (6–16 LT) with an evident asymmetry: In evening hours the speed drops significantly faster as you move away from noon in comparison with the morning hours. The vertical bars here and in subsequent figures show the standard error of the average, calculated as $\sigma/\sqrt{n}$ where σ is the standard deviation and n is the number of observations. The larger error bars for the average speed values for strong vortices is the result of having considerably fewer events in the calculation.

[17] The lower panel of Figure 7 shows the average eastward speed of vortices within each MLT hour for the total and for the strong vortices. The average vortex speed is directed westward in prenoon hours and eastward in the afternoon, changing sign at local noon. The average speed reaches a maximum of about 1 km/sec at 11–12 and 16–18 UT (9–10 and 14–16 MLT). This result confirms previous work which suggested that westward vortex movement should be dominant in prenoon sector and eastward in the after noon sector *Lühr and Blawert* [1994].

3.2. Relationship to Solar Wind Speed

[18] To investigate the relation between vortex occurrence and solar wind speed, the solar wind measurements were divided into 7 groups: $V_x < 350$ km/sec, V_x in range 350–400, 400–450, 450–500, 500–550, 550–600 and $V_x > 600$ where the measurements are in the GSE coordinate system. The number of vortices identified within these intervals was determined for each group separately. Within each bin, we divide the number of vortices observed by the total number of 20-minute observation intervals in order to obtain a uniform measure of the number of vortices/20 minutes interval.

[19] We computed the average number of vortices/20 minute universal time interval using the observations over the full 12 hour interval from 08 UT–20 UT corresponding to 06 MLT–18 MLT. We also computed the statistic separately for local time bins defined by the time intervals 8–12,12–16 and 16–20 UT (6–10, 10–14, 14–18 MLT). These intervals correspond to the morning, noon and evening sectors. Figure 8 shows the average number of vortices/20 minute interval as a function of solar wind speed for all (solid) and for strong (dotted line) vortices. The number of vortices significantly increases with increasing solar wind speed and this dependence is observed in all three local time sectors. The decrease in the number of all vortices observed in noon sector when $V_x > 550$ km/sec we believe to be an artifact (see explanation for Figure 7).

[20] The solar wind speed shows the highest correlation to vortex appearance in the noon sector. The probability of observing a strong vortex when $V_x > 600$ km/sec is about 14 times higher than when $V_x < 350$ km/sec. In the morning sector this ratio is about 8 and in the evening sector it is only 2.5.

[21] In Figure 8 we show the occurrence statistics without taking into account the strength of the vortices (except to show the statistics for the subset of strong vortices). To estimate the strength and number of vortices for a statistical investigation, we introduce the Vortex Activity Index (VAI) which is determined as the sum of the absolute value of the field-aligned current for all vortices observed during a 20-minute interval. Figure 9 shows the relation between solar wind speed and the vorticity activity index. The features observed in Figure 8 are even more evident in Figure 9. The noon sector shows the greatest slope and the evening sector shows the least slope.

[22] The solar wind velocity is not entirely along the $\hat{X}$ direction and we have examined the relationship between vortex strength (measured by the vorticity activity index) and the V_y and V_z solar wind components. We created the

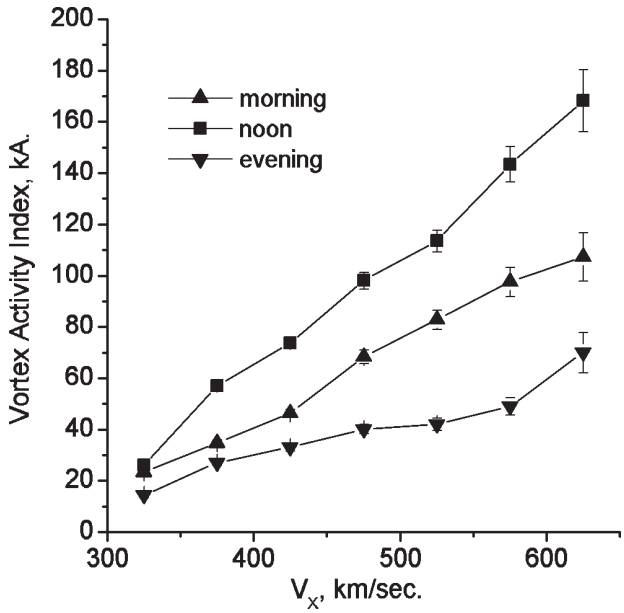

Figure 9. The average vortex activity index. (The VAI is defined as the sum of the absolute value of field-aligned current for all vortices within a 20-minute interval) as a function of solar wind speed V_x.

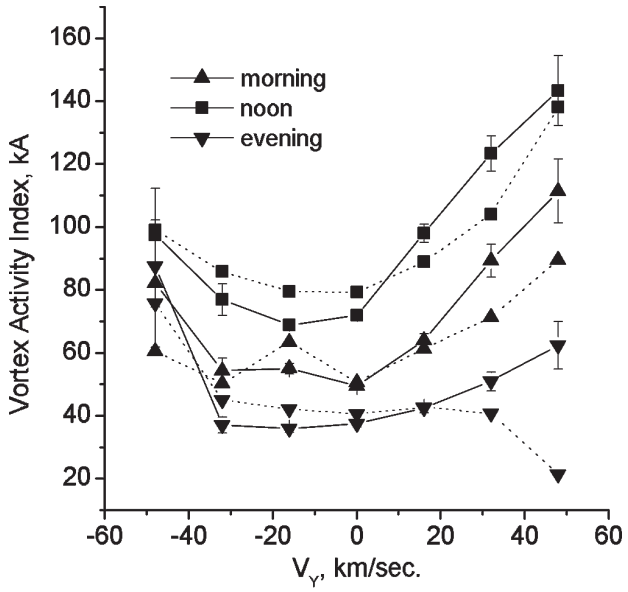

Figure 10. Average VAI per 20 minute interval as a function of solar wind aberration velocity V_y for the whole data set (solid lines). Dotted lines show results for groups where variation in V_x is limited to less that 25 km/s per bin in order to test the independence of the V_y result.

following velocity bins: $V_y < -40$ km/sec, $-40 < V_y < -24$, $-24 < V_y < -16$, $-16 < V_y < -8$, $-8 < V_y < 8$, $8 < V_y < 16$, $16 < V_y < 40$, $V_y > 40$ km/s and $V_z < -30$, $-30 < V_z < -18$, $-18 < V_z < -6$, $-6 < V_z < 6$, $6 < V_z < 18$, $18 < V_z < 30$, $V_z > 30$ km/s. The limits on the extreme bins were selected to give at least 400–500 points in those bins. The results for the V_y component are shown in Figure 10.

[23] Again we find a strong relationship between the vortex activity index and solar wind speed. We have tested this further by undertaking the same calculation using shorter time intervals (3-months and 6-months) and the results exhibited all of the features apparent in Figure 10.

[24] When the V_x component of the solar wind speed increases, it is reasonable to expect that the absolute value of the V_y component will increase also. Thus, we have tested to see if the V_y correlation shown in Figure 10 is independent. All events were divided into groups with V_x in the 25 km/s bins, (e.g. 350–375, 375–400, and so on up to 500 km/s). The correlation of vortex activity index versus V_y has been computed for each bin separately. Next, the vortex strength values for all groups with the same V_y have been averaged. The results are shown in Figure 10 by the dotted lines. The solid and dotted curves for the noon and morning sectors are nearly the same. The afternoon sector shows similar behavior for negative V_y, but somewhat different behavior for positive values. Since the V_x dependence has been removed in the dotted curves, we can conclude that the dependence on V_y is a real effect.

[25] For the V_z component (not shown) we find no correlation with VAI in the noon sector, but there may be some correlation in the morning and evening sectors. The vortex strength increases as the absolute value of V_z increases. Checking this relationship for shorter time intervals confirms the lack of correlation within the noon sector and confirms the correlation in the morning and evening sectors for winter months only. We find no correlation for summer months. We believe that this conclusion should remain tentative until checked in the data from other years and simultaneous summer and winter hemispheres can be examined.

3.3. Relationship With Interplanetary Magnetic Field

[26] For this investigation, all 20-minute intervals of solar wind observations have been divided into groups with $B < -5$nT, and 2nT bins (e.g. -5 to -3 nT, -3 to -1 nT, -1 to 1 nT, 1 to 3 nT, 3 to 5 nT, and $B > 5$ nT). We have examined relationships with the total field as well as with the Cartesian components in GSE and GSM coordinates. We present here the results obtained in GSM coordinates. The results for B_y are shown in Figure 11, the results for B_z are shown in Figure 12, and the results for B_x are shown in Figure 13. There is practically no relationship between VAI and the B_y component in all of the sectors. There is an increase in VAI associated with increasing negative B_z. The noon sector also shows a weak increase in VAI with negative B_x The dotted lines in Figures 11, 12 and 13 have been calculated to eliminate the effects of solar wind speed V_x in the manner described for Figure 10. The dotted lines confirm the lack of dependence on B_y and also confirm the dependence in the noon sector between VAI and negative B_z and negative B_x.

3.4. Relationship With the Variance of Solar Wind Parameters

[27] It might be thought that changes in the IMF or solar wind parameters trigger the formation of field-aligned currents which couple the outer magnetosphere to the ionosphere. Indeed, case studies indicate that changes in solar wind dynamic pressure or IMF orientation may initiate impulsive TCVs [e.g., *Friis-Christensen et al.*, 1988a].

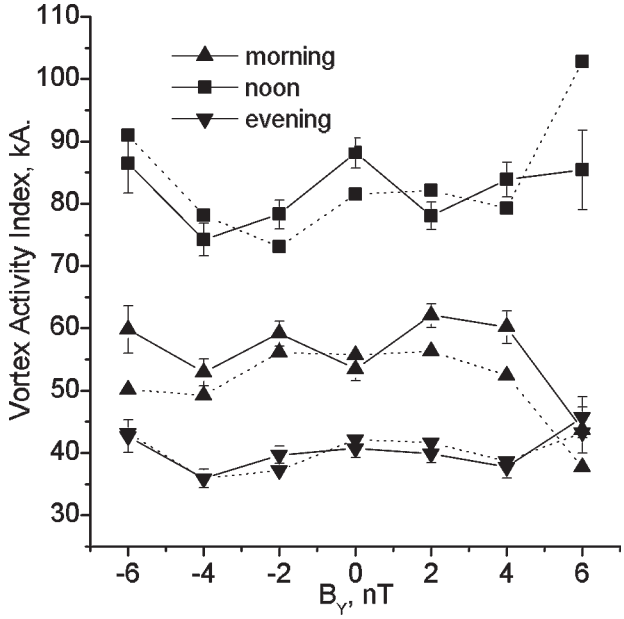

Figure 11. Average VAI per 20 minute interval as a function of IMF B_y GSM component for the whole data set (solid lines). Dotted lines show the results with the effects of solar wind V_x eliminated.

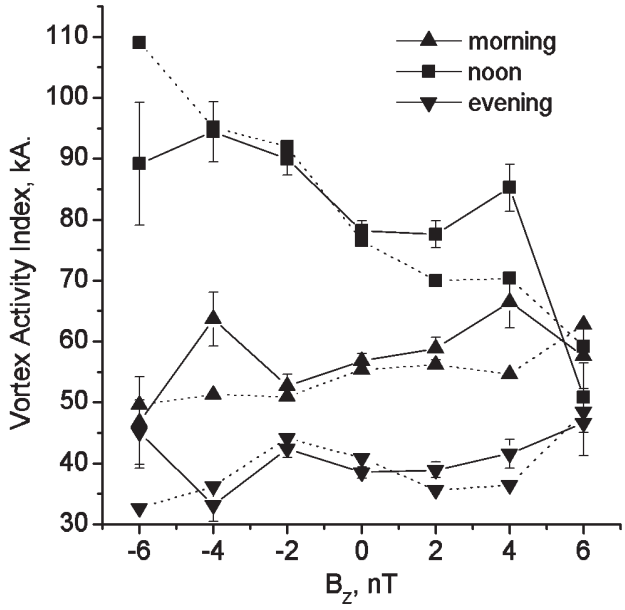

Figure 12. Average VAI per 20 minute interval as a function of IMF B_z GSM component for the whole data set (solid lines). Dotted lines show the results with the effects of solar wind V_x eliminated.

Thus, we undertake here a number of tests to examine the statistical relationship between TCVs and variability of the solar wind and IMF parameters.

[28] Figure 14 shows the relation between VAI and the average standard deviation ($\sigma(V_x)$) of the solar wind V_x during the 20-minute intervals (solid lines). There is a correlation between vortex strength and increasing $\sigma(V_x)$ observed in all sectors – noon evening and morning. The values of the vortex activity index are different in the three sectors, but they all increase about 2.4 times as the $\sigma(V_x)$ raises from 1 to 13 km/sec. We find, but do not show, that about the same dependence between VAI and the standard deviation of the V_y and V_z components exists. Figure 15 (solid lines) shows the relation between IMF B_y standard deviation and VAI. There is a clear correlation between the $\sigma(B_y)$ and the VAI: increasing $\sigma(B_y)$ leading to increasing VAI in all local time sectors.

[29] To test that the variability in the solar wind speed and IMF are separate, independent factors which correlate with the vortex activity index, it is again necessary to be sure that the standard deviation does not correlate with the main factor which influences vortex strength, i. e. solar wind speed V_x. Computing the correlation of V_x with the standard deviation of V_x, V_y, and V_z show that the correlation coefficients for all of them are about 0.5. This means that it is questionable whether the standard deviation of the solar wind speed V_x is independently correlated with VAI. Therefore, we again attempt to remove the dependence of V_x in the analysis. We have selected intervals when the solar wind speed is between 400 and 450 km/s and have conducted the same analysis on this subset. The results are shown by the dotted lines in Figure 14 and we see that there is no dependence of the VAI on $\sigma(V_x)$.

[30] The correlation coefficients between V_x and the standard deviation of B_x, B_y, and B_z are small but positive, ranging between 0.1 and 0.2. Nevertheless, we have undertaken a similar analysis for the IMF component standard deviations using intervals when the solar wind speed is between 400 and 450 km/s. The results for the standard deviation of the IMF B_y component are shown by the dotted lines in Figure 15. Similar results were found for the

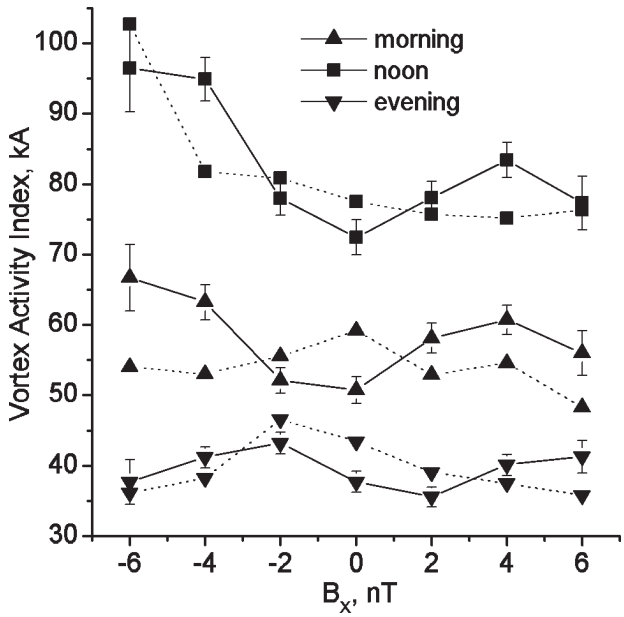

Figure 13. Average VAI per 20 minute interval as a function of IMF B_x GSM component for the whole data set (solid lines). Dotted lines show the results with the effects of solar wind V_x eliminated.

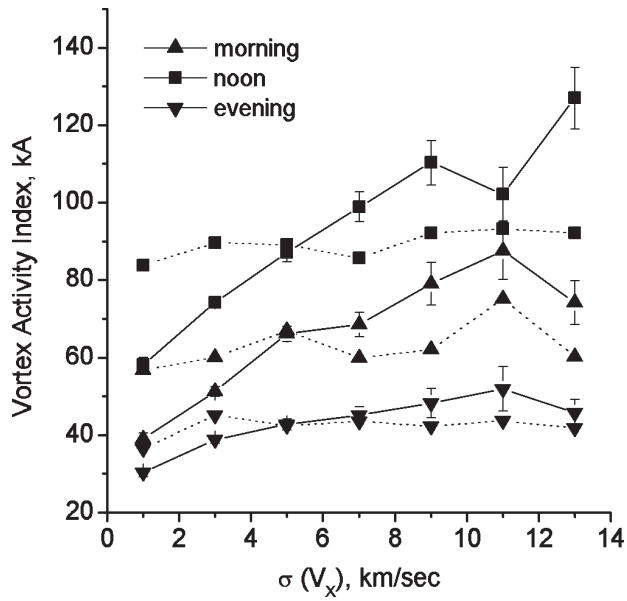

Figure 14. Average Vorticity Activity Index versus the average standard deviation of V_x for all 20-minute intervals (solid lines) separated by local time sector. Dotted lines show the relation of VAI to the average standard deviation of V_x for the subset of data when $400 < V_x < 450$ km/sec.

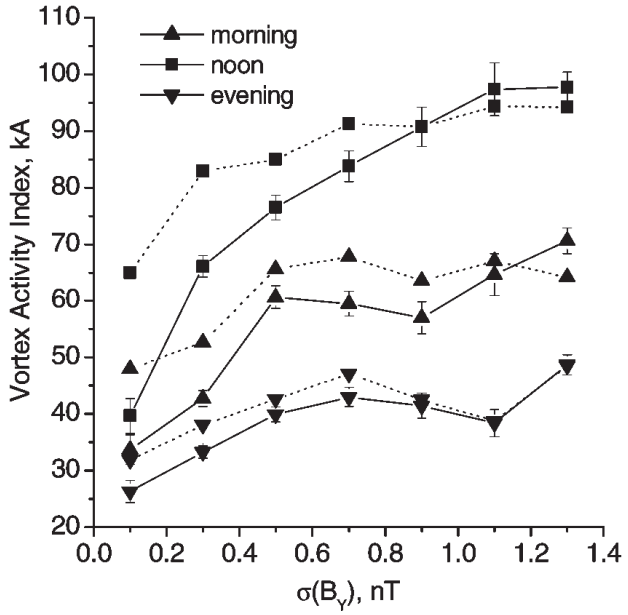

Figure 15. Average VAI versus the average standard deviation of IMF B_y GSM separated by local time sector. Dotted lines show the relation of VAI to the average standard deviation of B_y for the subset of events where the variation of V_x is limited to be between 400 and 450 km/s.

standard deviations of the other IMF components and the results indicate that variations in the IMF components show an independent correlation with increasing vortex strength in all local time sectors. The high correlation between the IMF components themselves makes the separation of the independent significance of each individual component difficult to determine and we have not tried to do so here.

3.5. Vortex Motion and Solar Wind Parameters

[31] As noted at the beginning of the paper, the average vortex motion has a very regular character: the zonal motion is directed to the west in the morning sector and to the east in the evening sector and the north-south motion directed northward. However, the standard deviation in the velocity is large, so there are a significant number of events in which the vortices move in the "wrong" direction. Such vortices have been observed by *McHenry et al.* [1990b] as well as others. Here we search for factors which may be related to the direction of vortex propagation. To do this we investigate the variations of the average vortex speed in relation to solar wind speed and magnetic field.

[32] Figure 16 shows the local time distribution of the eastward vortex speed V_e for IMF bins $B_y < -2$ nT, $-2 < B_y < 2$ nT, and $B_y > 2$nT. In the morning sector, the average vortex speed is westward with little dependence on B_y. In the evening sector the speed is eastward but decreases as B_y becomes positive. In the noon sector, positive B_y decreases the average eastward speed and negative B_y increases the eastward speed. The local time of the average speed reversal moves from about 11 LT to almost 13 LT as IMF B_y changes from negative to positive.

[33] To elucidate this further, we select vortices in the noon sector for which the absolute value of the eastward speed V_e is greater than 1 km/s. For these, we compute the

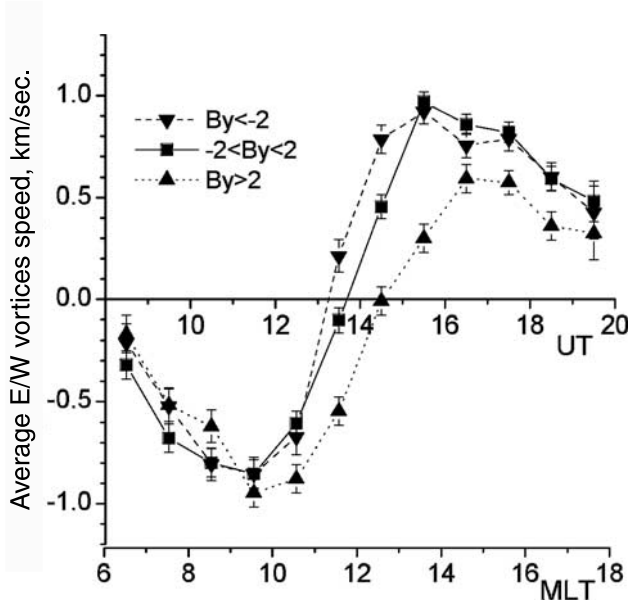

Figure 16. Local time distribution of average eastward vortex speed for all 20 minute intervals separated according to IMF B_y positive, zero, and negative.

percent of westward and eastward moving vortices as a function of IMF B_y. The results are shown in Figure 17. There is an almost linear dependence of vortex propagation direction on IMF B_y. When $B_y = -6$ nT only 25% of vortices are moving eastward (75% are moving westward) and the opposite situation when $B_y = 6$nT about 70% are moving eastward (30% are moving westward).

[34] As a further test, we have selected intervals during which $B_y > 2$ nT and $B_y < -2$ nT and the number of

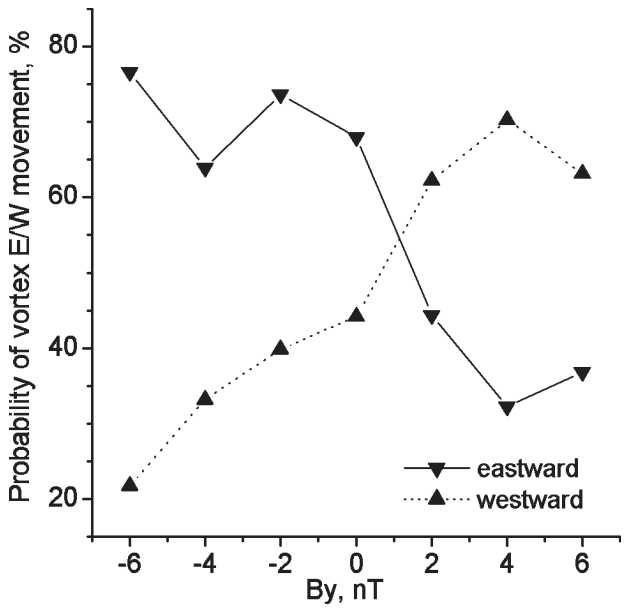

Figure 17. Probability distribution of eastward (solid line) or westward (dotted line) velocity in the noon sector for all vortices having a speed greater than 1 km/s as a function of IMF B_y GSM component.

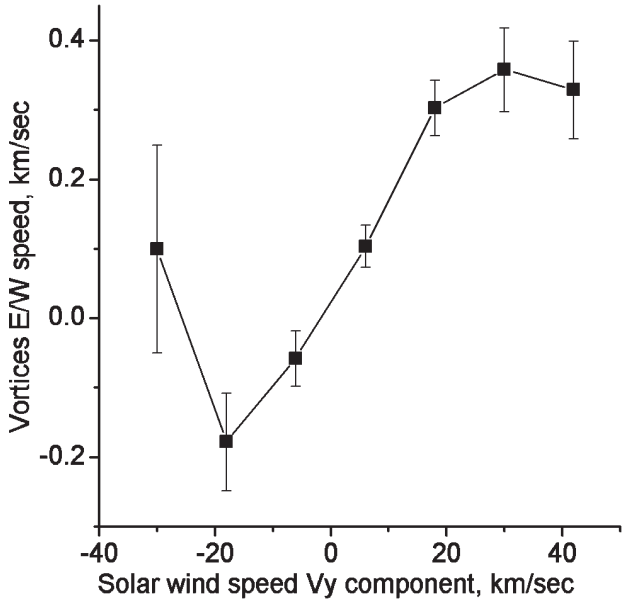

Figure 18. Average eastward vortex speed for all 20 minute intervals in the noon sector as a function of solar wind azimuth speed component V_y in GSE coordinates.

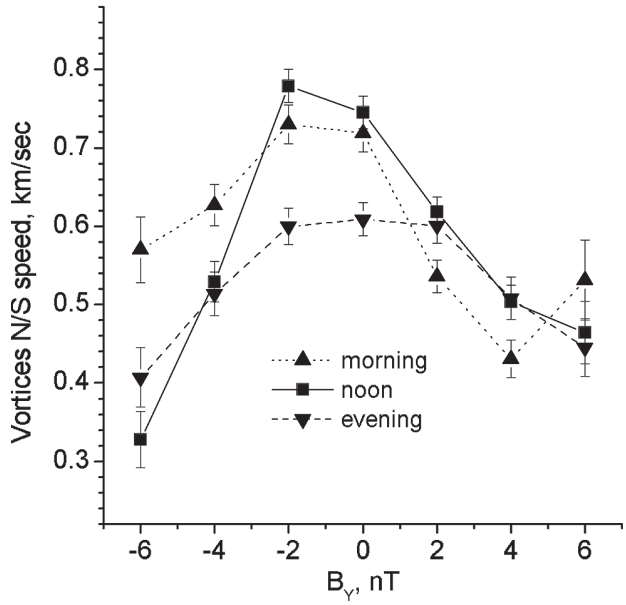

Figure 20. Average northward vortex speed for all 20 minute intervals separated according to local time sector as a function of IMF B_y GSM component.

eastward and westward moving vortices in the noon sector were counted. There were 2150 vortices when $B_y > 2$ nT and 41% of them moved eastward and 57% moved westward. For the case of $B_y < -2$nT there were 2447 vortices of which 63% moved eastward and 34% moved westward. While significant numbers are found to be moving in both directions either prenoon or postnoon, the statistic is consistent with that shown in Figure 7.

[35] We have investigated correlations of the east-west vortex speed with other solar wind parameters, but the only other significant correlation found is with the solar wind azimuthal velocity component V_y. This correlation exists in all local time sectors, but is strongest in the noon sector which is shown in Figure 18. Increasing solar wind V_y leads to increasing eastward vortex speed.

[36] Next we have investigated the influence of solar wind parameters on the northward component of vortex motion. The relationship between the vortex northward propagation velocity V_n and IMF B_z and B_y components is shown in Figures 19 and 20. There appears to be no influence of positive B_z on the northward propagation

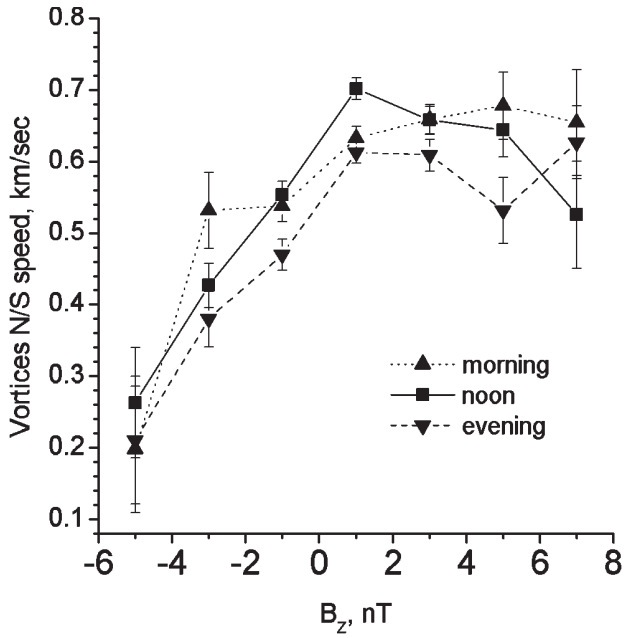

Figure 19. Average northward vortex speed for all 20 minute intervals separated according to local time sector as a function of IMF B_z GSM component.

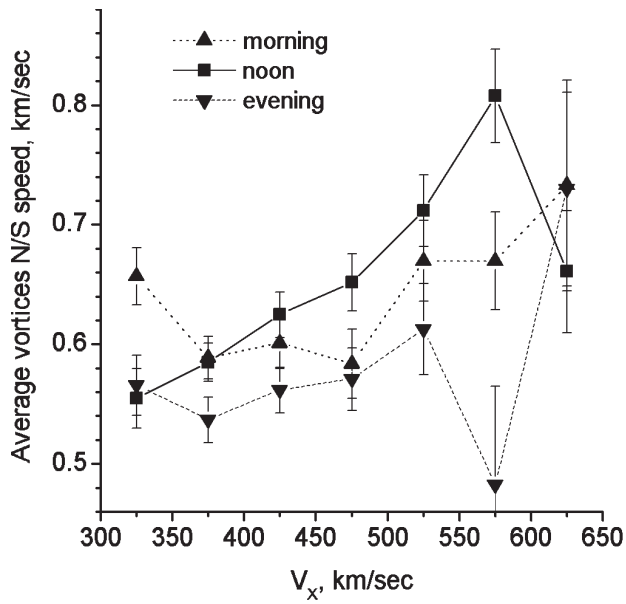

Figure 21. Average northward vortex speed for all 20 minute intervals separated according to local time sector as a function of solar wind velocity V_x.

velocity. The northward propagation velocity decreases with increasing negative IMF B_z. This dependence is similar in all local time sectors. For IMF B_y the relationship is quite different. Increasing absolute values of IMF B_y decreases the northward motion of the vortices. This is true in all sectors but the strongest relationship is shown in the noon sector. Thus, in the noon sector, a strong IMF B_y component not only increases the eastward or westward vortex speed but also diminishes the northward propagation.

[37] Figure 21 shows the average vortex northward propagation speed V_n as a function of solar wind speed V_x for the three sectors, evening, noon, and morning. In general there is increasing northward propagation speed with increasing solar wind speed V_x. The last point in the noon sector $V_x > 600$ km/s has few intervals so the uncertainty in this point is large.

4. Discussion and Conclusions

[38] We realize that one disadvantage of the above statistics is the mixture of TCVs which are likely generated by different mechanisms. We did not attempt to separate our data set according to TCV type (single impulsive events, continuous, etc). During the year, for example, is was possible to select only 90 single TCV events which were single vortices separated by at least 30 minutes from another vortex. Analysis of these events yielded too great a scatter to obtain reliable results.

[39] We did form a subset of large amplitude events which we investigated separately. The results obtained for this subset, however, are generally similar to the results obtained using the whole data set. In some cases for positive or negative IMF B_z we did find some differences as discussed above. We believe that the results presented here are valid for the most common multiple traveling vortex events.

[40] It is also well known that dayside Pc5 pulsation trains at cusp latitudes include and overlap the pulsations which form the class of TCVs which have been investigated here. ULF power in the Pc5 range has been investigated by many authors. The Pc5 occurrence and intensity observed near dawn is well correlated with increased solar wind velocity both in the equatorial outer magnetosphere and on the ground [*Junginger and Baumjohann*, 1988; *Kokubun et al.*, 1989; *Greenstadt et al.*, 1979; *Glassmeier et al.*, 1989]. ULF pulsation energy at cusp latitudes near local noon has also been found to be enhanced during intervals of increased solar wind velocity [*Yumoto et al.*, 1987; *Wolfe et al.*, 1994; *Engebretson et al.*, 1995]. *Engebretson et al.* [1998] show that Pc5 power integrated over a six-hour period measured in both local morning auroral latitudes and local noon cusp latitudes show a power-law dependence on the solar wind velocity, but with different exponents. Variations in the remaining Pc5 power appear due to temporal patterns related to the response to solar wind high speed streams. For example, the power is strongest at the leading edge of high speed streams and subsequently decreases more rapidly than the solar wind velocity. The TCVs selected in this study comprise a significant portion of the class of Pc5 pulsations and the strong relationship to solar wind velocity is consistent with the Pc5 statistics.

[41] We also realize that many other relationships between various TCV parameters and the solar wind and IMF parameters are possible, and we continue to look at them. We present here a set of rather basic relationships and we may show more relationships in another publication at a later time if significant other relationships are obtained.

[42] The TCV occurrence probability shown in Figure 7 exhibits a broad distribution from 08 to 16 LT with a weak maximum slightly after noon. This differs from previous statistical results which show a maximum probability at about 09 LT [*Glassmeier et al.*, 1989], 14 LT [*McHenry et al.*, 1990b], 09 and 14 MLT [*Lanzerotti et al.*, 1991], but agree with *Lin et al.* [1995]. The *Lin et al.* [1995] study was able to use a small amplitude criteria in their event selection, and we also utilize a smaller amplitude criteria than many past studies. This may explain the lack of a double peaked pattern with noon minimum. An examination of the local time distribution of only the large amplitude events shows a larger integrated area under the curve in the prenoon sector (Figure 7). This may support the conclusion by *Sibeck and Korotova* [1996] that events attain their greatest amplitude in the prenoon local time sector. The *Sibeck and Korotova* [1996] statistic, however, is based upon an analysis of magnetic impulse events, and while our event selection contains impulsive events, the majority of events in our study consist of multiple traveling vortices which would not be considered impulsive.

[43] The features of the east-west vortex speed local time distribution are in general agreement with previous studies which have reported antisunward vortex motion, however, the average speed obtained here (about 1km/s) is lower than the typical speeds reported elsewhere (3–5 km/s). There may be a few reasons for that. We used a fixed size vortex model and real vortices may be larger in the east-west dimension than our model dimension. We also used an ideal induction effect approximation which may also be different from the real induction effect, with the result that the distance between the meridian chain of measurements and the modeled vortex center may be shorter than the real distance. This would produce a lower absolute value of the speed (by a factor up to 2) but not change the direction. Finally, the speed distribution function is rather wide with a standard deviation of about 1km/s. In each local time sector there are vortices moving in both directions. If we compute the average speed using only westward (in the morning sector) and eastward (in the evening sector) moving vortices, we obtain values around 1.6 km/s. Multiplying this by 2 gives average values within the 3–3.5 Km/s range which is in agreement with earlier reports. The accuracy of this statistic may not be well resolved using the fitting procedure in this study, and should be checked using a phase measurement between longitudinally spaced stations.

[44] There may be two explanations of the observed northward propagation of vortices. The first is that the observed motion is real, and the second is that it is apparent because the vortices are elongated and tilted with respect to the east-west direction and the equatorward side leads the vortex motion as noted by *McHenry et al.* [1988]. However, we believe that the northward motion is real. If this were merely an apparent northward motion due to the tilt of the vortex ellipse axis and a purely east-west motion, the dependence on solar wind parameters should be the same

for both east-west and northward propagation. The different dependencies of the northward and eastward speed on solar wind parameters (Figures 21, 19, and 20) support the point that the northward speed component of the motion is real. In addition, the northward component of the velocity should be better resolved by the fitting procedure since we are utilizing a dense north-south chain of stations for the analysis.

[45] Comparison of Figures 9, 10, 11, 12, 13, 14, and 15 show that the main factor influencing the VAI index is the solar wind speed V_x, in agreement with result of *Olson* [1986], and *Wolfe et al.* [1987]. Increasing solar wind speed increases the vortex occurrence, as well as vortex intensity. The dependence is strongest in the noon sector, followed by the morning and evening sectors.

[46] We computed the relation between the solar wind dynamic pressure and VAI obtaining a relation which resembles $VAI \propto (\rho V^2)^{1/2}$. This suggests that the primary relationship is between VAI and V. It is also interesting to note that the orbital motion of the Earth around the sun produces an aberration in the observed solar wind radial velocity of 27 km/s. Only when the solar wind GSE speed is -27 km/s will there be no V_y measured according to the Earth. This value is quite close to the minima in the curves shown in Figure 10, so the minimum in VAI is observed when the V_y component in the system moving with the Earth is near zero. In judging the relative importance of the V_x and V_y components, it seems that the V_x component is more significant. In the noon sector, VAI increases 7 times as a function of V_x, and only 2 times as a function of V_y. However, taking into account that the range of variation of V_x is about 300 km/s while the range of variation of V_y is only 70 km/s, they, in fact, become comparable.

[47] The IMF B_z component has a nearly comparable influence on VAI as the solar wind speed, however, this is observed primarily in the noon sector. The final factor which we have found to influence the VAI is the standard deviation of the magnetic field.

[48] The relationship between solar wind speed and the vortex activity index supports the Kelvin-Helmholtz instability as a source of TCVs. In particular, the V_y component could produce a speed shear along the dayside magnetopause near the subsolar meridian. The noon sector dependence of the eastward vortex propagation speed on the solar wind V_y and the northward propagation speed on V_x also are consistent with the Kelvin-Helmholtz mechanism.

[49] On the other hand, the relation between VAI and the standard deviation of the magnetic field, as well as the increased VAI with IMF $B_z < 0$ supports a relationship to changes in reconnection or to transient localized reconnection (FTEs). Reconnection is more likely as the IMF becomes more southward, and changes in reconnection are more likely as the standard deviation of the IMF increases. The relationship between vortex motion with IMF B_z (Figure 19) and with B_y (Figures 16 and 17) components also support the magnetic reconnection mechanism since the tension on the reconnected field lines would cause them to move westward for positive IMF B_y and eastward for negative IMF B_y.

[50] We also find a good relationship between the standard deviation of the solar wind velocity $\sigma(V_x)$ and the VAI (Figure 14, solid lines). The correlation between vortex strength and increasing standard deviation is observed in all local time sectors. This result is consistent with a pressure pulse generation mechanism. However, since the solar wind V_x correlates with $\sigma(V_x)$, it is necessary to test that $\sigma(V_x)$ is independently correlated with VAI. In doing this test shown with dotted lines in Figure 14 we find the surprising result that there is no dependence of VAI on $\sigma(V_x)$ which reduces support for the pressure pulse generation mechanism which has been the primary mechanism thought to generate impulsive events. It is possible that our collection of events does not contain sufficient numbers of impulsive events to resolve this effect. Also, pressure variations in the magnetosheath are produced by bow shock interactions which we have not investigated. Nevertheless, we note that other studies could not find a consistent relationship between TCVs and solar wind pressure variations [*Sitar et al.*, 1996; *Bering et al.*, 1990]. So, while pressure variations are intuitively thought to be a primary generation mechanism for TCVs, there is little statistical evidence to support this mechanism at this time. Generation mechanisms related to changes in reconnection and to shear flow instabilities (e.g. Kelvin Helmholtz) have the greatest statistical support.

[51] **Acknowledgments.** This work is supported by NSF Grants ATM-9801941 and 9628706. We also thank the International Space Science Institute for hosting the Workshop on Traveling Convection Vortices which helped to develop this work.

[52] Janet G. Luhmann thanks the referees for their assistance in evaluating this paper.

References

Banks, R. J., Geomagnetic variations and the electric conductivity of the upper mantle, *Geophys. J. R. Astron. Soc.*, *17*, 457, 1969.

Bering, E. A., L. J. Lanzerotti, J. R. Benbrook, Z. M. Lin, C. G. Maclennan, A. Wolfe, R. E. Lopez, and E. Friis-Christensen, Solar wind properties observed during high-latitude impulsive perturbation events, *Geophys. Res. Lett.*, *17*, 579, 1990.

Clauer, C. R., and A. J. Ridley, Ionospheric observations of magnetospheric low latitude boundary layer waves on August 4, 1991, *J. Geophys. Res.*, *100*, 21,873, 1995.

Engebretson, M., W. J. Hughes, J. L. Alford, E. Zesta, L. J. Cahill Jr., R. L. Arnoldy, and G. D. Reeves, Magnetometer array for cusp and clef studies observations of the spatial extent of broadband ULF magnetic pulsations at cusp/cleft latitudes, *J. Geophys. Res.*, *100*, 19,371, 1995.

Engebretson, M., K.-H. Glassmeier, M. Stellmacher, W. J. Hughes, and H. Lühr, The dependence of high-latitude Pc5 wave power on solar wind velocity and on the phase of high-speed solar wind streams, *J. Geophys. Res.*, *103*, 26,271, 1998.

Friis-Christensen, E., M. A. McHenry, C. R. Clauer, and S. Vennerstrøm, Ionospheric travelling convection vorticies observed near the polar cleft: A triggered response to sudden changes in the solar wind, *Geophys. Res. Lett.*, *15*, 253, 1988a.

Friis-Christensen, E., S. Vennerstrøm, C. Clauer, and M. A. McHenry, Irregular magnetic pulsations in the polar cleft caused by traveling ionospheric current vortices, *Adv. Space Res.*, *8*(9–10), 311, 1988b.

Glassmeier, K.-H., Traveling magnetospheric convection twin-vortices: Observations and theory, *Ann. Geophys.*, *10*, 547, 1992.

Glassmeier, K.-H., and C. Heppner, Traveling magnetospheric convection twin vortices: Another case study, global characteristics, and a model, *J. Geophys. Res.*, *97*, 3977, 1992.

Glassmeier, K., M. Hönisch, and J. Untiedt, Ground-based and satellite observations of travelling magnetospheric convection twin vorticies, *J. Geophys. Res.*, *94*, 2520, 1989.

Goertz, C., E. Nielsen, A. Korth, K.-H. Glassmeier, C. Haldoups, P. Hoeg, and D. Hayward, Observations of a possible ground signature of flux transfer events, *J. Geophys. Res.*, *90*, 3069, 1985.

Greenstadt, E. W., J. V. Olson, P. D. Loewen, H. J. Singer, and C. T. Russell, Correlation of Pc3, 4 and 5 activity with solar wind speed, *J. Geophys. Res.*, *84*, 6694, 1979.

Heikkila, W., T. Stockflet-Jorgensen, L. J. Lanzerotti, and C. G. Maclennan, A transient auroral event on the dayside, *J. Geophys. Res.*, *94*, 15,291, 1989.

Junginger, H., and W. Baumjohann, Dayside long period magnetospheric pulsations: Solar wind dependence, *J. Geophys. Res.*, *93*, 877, 1988.

Kokubun, S., N. Erickson, T. A. Fritz, and R. L. McPherron, Local time asymmetry of pc4-5 pulsations and associated particle modulations at synchronous orbit, *J. Geophys. Res.*, *94*, 6607, 1989.

Lanzerotti, L., R. D. Hunsucker, D. Rice, L. Lee, A. Wolfe, C. Maclennan, and L. Medford, Ionosphere and ground-based response to field aligned currents near the magnetospheric cusp regions, *J. Geophys. Res.*, *92*, 7739, 1987.

Lanzerotti, L., R. Konik, A. Wolf, D. Venkatesan, and C. Maclennan, Cusp-latitude magnetic impulse events, 1, Occurrence statistics, *J. Geophys. Res.*, *96*, 14,009, 1991.

Lin, Z. M., E. A. Bering, J. R. Benbrook, B. Lao, L. J. Lanzerotti, C. G. MacLennan, A. N. Wolfe, and E. Friis-Christensen, Statistical studies of impulsive event at high latitudes, *J. Geophys. Res.*, *100*, 7553, 1995.

Lühr, H., and W. Blawert, Ground signature of travelling convection vortices, in *Solar Wind Sources of Magnetospheric Ultra-Low-Frequency Waves, Geophys. Monogr. Ser.*, vol. 64, edited by M. Engebretson, K. Takahashi, and M. Scholer, p. 231, AGU, Washington, D.C., 1994.

Lühr, H., W. Blawert, and H. Todd, The ionospheric plasma flow and current patterns of travelling convection vortices: A case study, *J. Atmos. Terr. Phys.*, *55*, 1717, 1993.

Lühr, H., M. Lockwood, P. E. Sandholt, T. L. Hansen, and T. Moretto, Multi-instrument ground-based observations of a travelling convection vortices event, *Ann. Geophys.*, *14*, 162, 1996.

McHenry, M. A., Ground signatures of dayside magnetospheric boundary layer phenomena, Ph.D. thesis, Stanford Univ., Stanford, Calif., 1989.

McHenry, M. A., and C. R. Clauer, Modeled ground magnetic signatures of flux transfer events, *J. Geophys. Res.*, *92*, 11,231, 1987.

McHenry, M. A., C. R. Clauer, E. Friis-Christensen, and J. D. Kelly, Observations of ionospheric convection vortices: Signatures of momentum transfer, *Adv. Space Res.*, *8*(9–10), 315, 1988.

McHenry, M. A., C. R. Clauer, and E. Friis-Christensen, Relationship of solar wind parameters to continuous dayside, high latitude traveling ionospheric vortices, *J. Geophys. Res.*, *95*, 15,007, 1990a.

McHenry, M. A., C. R. Clauer, E. Friis-Christensen, P. T. Newell, and J. D. Kelly, Ground observations of magnetospheric boundary layer phenomena, *J. Geophys. Res.*, *95*, 14,995, 1990b.

Olson, J. V., ULF signatures of the polar cusp, *J. Geophys. Res.*, *91*, 10,055, 1986.

Pu, Z., and M. G. Kivelson, Kelvin-Helmholtz instability at the magnetopause: Solution for compressible plasmas, *J. Geophys. Res.*, *88*, 841, 1983.

Ridley, A. J., Estimations of the uncertainty in timing the relationship between magnetospheric and solar wind processes, *J. Atmos. Sol. Terr. Phys.*, *62*, 757, 2000.

Ridley, A. J., T. Moretto, P. Ernstrøm, and C. Clauer, Global analysis of three traveling convection vortex events during the Nov. 93 storm using the assimilative mapping of ionospheric electrodynamics technique, *J. Geophys. Res.*, *103*, 26,349, 1998.

Sibeck, D. G., A model for the transient magnetospheric response to sudden solar wind dynamic pressure variations, *J. Geophys. Res.*, *95*, 3755, 1990.

Sibeck, D. G., and G. I. Korotova, Occurrence patterns for transient magnetic field signatures at high latitudes, *J. Geophys. Res.*, *101*, 13,413, 1996.

Sitar, R. J., and C. R. Clauer, Ground magnetic response to sudden changes in the interplanetary magnetic field orientation, *J. Geophys. Res.*, *104*, 28,343, 1999.

Sitar, R. J., C. R. Clauer, and E. Friis-Christensen, High latitude ground based response to sudden changes in solar wind dynamic pressure, *J. Geophys. Res.*, *101*, 27,001, 1996.

Wolfe, A., E. Kamen, L. J. Lanzerotti, C. G. Maclennan, J. F. Bamber, and D. Venkatesan, ULF geomagnetic power at cusp latitudes in response to upstream solar wind conditions, *J. Geophys. Res.*, *92*, 168, 1987.

Wolfe, A., R. D. Kelman, S. E. Warren, C. G. Maclennan, and L. J. Lanzerotti, Hydromagnetic frequency spectra in the high-latitude quiet magnetosphere, in *Solar Wind Sources of Magnetospheric Ultra-Low-Frequency Waves, Geophys. Monogr. Ser.*, vol. 64, edited by M. J. Engebretson, K. Takahashi, and M. Scholer, p. 377, AGU, Washington, D.C., 1994.

Yumoto, K., A. Wolfe, T. Terasawa, E. L. Kamen, and L. J. Lanzerotti, Dependence of pc2 magnetic energy spectra at South Pole on upstream solar wind parameters, *J. Geophys. Res.*, *92*, 12,437, 1987.

C. R. Clauer and V. G. Petrov, Space Physics Research Laboratory, University of Michigan, 2455 Hayward, Ann Arbor, MI 48109-2143, USA. (bob.clauer@umich.edu)